Improving musculoskeletal model scaling using an anatomical atlas: the importance of gender and anthropometric similarity to quantify joint reaction forces

Ziyun Ding[*], **Chui K. Tsang**, **Daniel Nolte**, **Angela E. Kedgley**, **Anthony M. J. Bull**
Department of Bioengineering, Imperial College London, SW7 2AZ, United Kingdom

Abstract

Objective—The accuracy of a musculoskeletal model relies heavily on the implementation of the underlying anatomical dataset. Linear scaling of a generic model, despite being time and cost-efficient, produces substantial errors as it does not account for gender differences and inter-individual anatomical variations. The hypothesis of this study is that linear scaling to a musculoskeletal model with gender and anthropometric similarity to the individual subject produces similar results to the ones that can be obtained from a subject-specific model.

Methods—A lower limb musculoskeletal anatomical atlas was developed consisting of ten datasets derived from magnetic resonance imaging of healthy subjects and an additional generic dataset from the literature. Predicted muscle activation and joint reaction force were compared with electromyography and literature data. Regressions based on gender and anthropometry were used to identify the use of atlas.

Results—Primary predictors of differences for the joint reaction force predictions were mass difference for the ankle ($p<0.001$) and length difference for the knee and hip (p 0.017). Gender difference accounted for an additional 3% of the variance (p 0.039). Joint reaction force differences at the ankle, knee and hip were reduced by between 50% and 67% ($p=0.005$) when using a musculoskeletal model with the same gender and similar anthropometry in comparison with a generic model.

Conclusion—Linear scaling with gender and anthropometric similarity can improve joint reaction force predictions in comparison with a scaled generic model.

Significance—The scaling approach and atlas presented can improve the fidelity and utility of musculoskeletal models for subject-specific applications.

Index Terms

anatomical atlas; musculoskeletal model; scaling; anthropometry; magnetic resonance imaging

[*]correspondence z.ding@imperial.ac.uk.

I Introduction

Computational modelling and simulation of the musculoskeletal system can be used to address biomechanical questions, including those that require information that is not amenable to direct measurement, such as muscle forces and articular, or joint, loading. This type of information is essential for clinical applications, including: designing assistive devices [1], planning rehabilitative treatments [2], [3], analysing pathology such as osteoarthritis [4], designing implants [5], and the prevention of injuries [6].

The quantification of muscle forces and articular loading requires a detailed description of musculoskeletal geometry in the musculoskeletal model that is used to mathematically model the skeletal bones, joint articulations and musculotendon actuators. The lower limb model created by Delp et al. has been used extensively, and its underlying dataset is an amalgamation of two classic studies using measurements of five cadaver subjects [7] that has since been altered and refined [8], [9]. This generic model is used to investigate the general features of musculoskeletal design [8] and has been extended to include large numbers of additional subject measurements, such as incorporating variations in muscle volume and length [10], [11]. Klein Horsman et al. [12] published the first complete dataset that was based on the geometrical measurement of a single cadaveric specimen (male, age 77 years, mass 105 kg, height 1.74 m), and others have followed this approach (Carbone et al. [13]; male cadaver, age 85 years, mass 45 kg).

Linear scaling of generic models is the most time and cost efficient way in the clinical setting of representing an individual's musculoskeletal geometry [14] – [16]. In this approach simple measurements of anthropometry such as body mass and limb lengths are used to scale the documented generic dataset to the individual subject [16], [17]. However, the generic models currently available (presented in TABLE I) do not enable gender and inter-individual anatomical variations to be accounted for [18], [19]. Such variations in human anatomy cannot be extrapolated comfortably from a single model and substantial errors have been reported when generic models are used, through scaling, to represent individual subjects [20] – [23].

Three-dimensional reconstructions of high-resolution magnetic resonance imaging (MRI) can accurately reproduce bone and muscle geometry [24] and accurately quantifies moment arm and muscle length [25]. Thus, MRI can be used to generate an anatomical dataset of in vivo subjects; such subject-specific models improve musculoskeletal modelling accuracy when compared to generic scaling [26], [27]. However, creating such a dataset for every subject for which musculoskeletal modelling is used is time and technology intensive, and thus is not in widely clinical use. The hypothesis of this study is that linear scaling to a musculoskeletal model with gender and anthropometric similarity to the individual subject produce similar results to the ones that can be obtained from a subject-specific model. This hypothesis is tested through: first, developing a lower limb musculoskeletal anatomical database, or atlas, consisting of datasets derived from MRI and a generic dataset from the literature; secondly, quantifying the discrepancies from scaled models where the outputs from the personalised, subject-specific musculoskeletal model are considered as a reference [28] – [30]; and finally, establishing any relationship between discrepancies of scaled models

and the discrepancies from the underlying datasets to the modelled subject to define the use of the atlas in situations where it is impractical to create a subject-specific model to quantify joint reaction forces.

II   Methods

This study was approved by the NHS Research Ethics Committee and the Imperial College Research Ethics Committee. Written informed consent was obtained from all ten healthy subjects, covering a wide range of body heights, all with no lower limb musculoskeletal conditions (TABLE II).

A   MRI-based musculoskeletal atlas

MRIs of each subject were acquired. T1 weighted axial spin echo scans were performed with the subjects lying supine with extended knees using a 3.0 T MRI scanner (MAGNETROM Verio, Siemens, Germany). Six axial image series were taken contiguously from the fifth lumbar vertebra to the distal end of the limb with the following settings: field of view 450×450 mm^2, acquisition matrix $= 320 \times 320$, axial plane resolution 1.406 mm $\times 1.406$ mm, slice thickness 1 mm. The total acquisition time per subject was approximately 40 minutes.

Each series of axial images was automatically registered, providing a field of view of the entire lower limbs. 3D bone surfaces of the pelvis and the right femur, tibia/fibula, patella and foot (calcaneus, talus and navicular bones for all subjects, and metatarsal bones for six subjects) were reconstructed based on manual segmentation of bone contours in the axial images.

Twenty-one anatomical landmarks were manually digitised on the bone surface. The landmarks were used to construct the local coordinate systems of the lower limb, as described by the Standardisation and Terminology committee of the International Society of Biomechanics [32]. Tibiofemoral contact points were digitised as the most distal ends of the medial and/lateral femoral condyles.

The joint parameters were identified by manually fitting geometrical objects to the articular surfaces. The following joint parameters were identified: hip joint centre (centre of a sphere fitted to the femoral head, Fig. 1a); knee joint centre (midpoint of the central axis of a cylinder fitted to the boundaries of both femoral condyles, Fig. 1b); and ankle joint centre (centre of a sphere fitted to the talar dome, Fig. 1c). The fitting error, the root mean squared distance between a set of 50 digitised points on the articular surface to the surface of the fitted object, was 0.7 ($\pm$ standard deviation 0.3) mm, 1.7 ($\pm$ 0.6) mm, and 1.8 ($\pm$ 1.0) mm for the hip, knee and ankle joints, respectively. The fitting error in each dataset is reported in the supplementary datasets.

Muscle and ligament lines-of-action were described by the origin, via and insertion points. Following the topology of the generic dataset of Klein Horsman et al. [12], which has been implemented in this atlas, lines-of-action of 163 muscle elements and the patella ligament were measured in the MR images (Fig. 1d), where the origins of psoas were estimated based

on the measured length of the fifth lumbar vertebra and the intervertebral disc. For gastrocnemius and iliopsoas that are free to glide over the underlying bone of the femoral condyles and pubis of the pelvis, two wrapping cylinders were defined in the generic dataset. These cylinders were manually identified in MR images based on the curved muscle lines-of-action of gastrocnemius and iliopsoas and the segmented bone surface. The fitting error, the root mean squared distance between a set of 50 points digitised on the posterior surface of the femoral condyles and the superior surface of the pubic ramus to the cylindrical surface, was 1.5 ($\pm$ 0.2) mm and 1.3 ($\pm$ 0.2) mm, respectively. The fitting error in each dataset is reported in the supplementary datasets.

Segmentation and digitisation of MR images were performed using Mimics (Mimics 17.0, Materialise, Belgium) by two experienced operators. On completion, one operator reviewed and refined all segmentation and digitisation to ensure consistency across the atlas. The intra- and inter-operator reliability in digitisation of the anatomical landmarks and tibiofemoral contact points was tested for a subset of six subjects (three male, three female). The intraclass correlation coefficient (ICC, two-way mixed effects, absolute agreement) was higher than 0.99 and the intra- and inter-operator differences are reported in supplementary Fig. A.1.

As shown in the literature, the whole lower limb muscle volume is correlated with the subject's height-mass product and the distribution of each individual muscle volume is well preserved across a group of healthy young subjects [11]. According to the equation in [11] the whole lower limb muscle volume (V_{lm}) of each subject was calculated:

$$V_{lm} = 47 \times m \times h + 1285 \tag{1}$$

where m is subject mass in kg and h is subject height in metres.

The muscle volume (V_m) was proportional to the whole lower limb muscle volume and the muscle length (L_m) was proportional to the lower limb length, according to the mean value from the literature [11]. Muscle physiological cross-sectional area (PCSA) was calculated as:

$$\text{PCSA} = \frac{V_m \cos \theta}{L_m \times \frac{L_f}{L_m} \times \frac{2.7}{L_s}} \tag{2}$$

where θ is the pennation angle; $\frac{L_f}{L_m}$ is fibre length to muscle length ratio [10]; and $\frac{2.7}{L_s}$ is the ratio of optimal sarcomere length to the sarcomere length in μm [33].

Muscle parameters of a representative subject are presented in TABLE III. Ten MR-based anatomical datasets (including coordinates of bony landmarks, joint centres/axes, contact points, lines-of-action of muscles and ligament, wrapping object parameters and muscle parameters) are available in the supplementary datasets.

B Gait data collection

Within six months (mean ± standard deviation [range]: 3.1 ± 2.3 [0.1 - 6.0] months) from MR imaging acquisition, gait data from the same subjects were acquired using a 10-camera VICON motion analysis system (Oxford Metrics Group, UK) with two force plates (Kistler Type 9286B, Kistler Instrumente AG, Winterthur, Switzerland). The marker set comprised anatomical landmarks of the whole lower limbs (markers on the anterior/posterior superior iliac spine, medial/lateral femoral epicondyles, medial/lateral malleolus, the second/fifth metatarsal and the heel) as well as clusters of three markers each for the thighs and shanks [34]. Subjects were instructed to perform six level walking trials at a self-selected comfortable speed (1.25 ± 0.15 [1.03 - 1.41] m/s). The final three trials were selected for analysis. Surface electromyography (EMG; Myon 320, Myon AG., Switzerland) during gait was recorded at 1000 Hz from eight muscles: gluteus medius, rectus femoris, vastus lateralis, vastus medialis, biceps femoris long head (LH), semitendinosus, soleus and tibialis anterior. The electrodes were aligned parallel to the muscle fibres over the muscle belly, as described in the literature [35], [36]. Prior to electrode placement, the skin was shaved and cleaned with alcohol wipes. Recorded EMG signals were corrected for offset, high-pass filtered at 30 Hz using a zero phase-lag, four order Butterworth filter and rectified. The rectified signals were then low-pass filtered at 10 Hz [37].

C Lower limb musculoskeletal model

A lower limb musculoskeletal model FreeBody V2.1 was used to quantify forces during gait [38], [39]. It consists of four rigid segments (foot, shank, thigh and pelvis), articulated by ankle, knee and hip joints, actuated by 163 lower limb muscle elements and the patellar ligament. The ankle and knee joints each possess six degrees of freedom (DOFs, a combination of 3DOFs planar joint and 3DOFs spherical joint), and, in this use of the model, the hip joint possesses three rotational DOFs (a spherical joint). The position and orientation of each rigid segment was constructed based on the measured kinematics using the method in [40], with a constraint to the hip joint [39]. The net joint force and moment was calculated using wrench notation in the inverse dynamic method [41]. Afterwards, muscle forces and resultant articulated contact forces across the ankle, knee and hip joints were calculated using a one-step static optimisation [42] by minimising the sum of cubed muscle activations [43]. The optimisation model is formulated, as below (3):

$$min \sum_{m=1}^{163} \left(\frac{f_m}{f_{max_m}} \right)^3 \text{ subject to}$$

$$\left[\begin{array}{c} \sum_{l=1}^{L} f_l \cdot \boldsymbol{n}_{li} - \sum_{k=1}^{K} f_k \cdot \boldsymbol{n}_{k(i-1)} + \boldsymbol{J}_i - \boldsymbol{J}_{i-1} \\ \sum_{l=1}^{L} f_l \cdot \boldsymbol{n}_{li} \times r_{li} - \sum_{k=1}^{K} f_k \cdot \boldsymbol{n}_{k(i-1)} \times r_{k(i-1)} - \tilde{d}_i \times \boldsymbol{J}_{i-1} \end{array} \right]$$
$$= \left[\begin{array}{cc} M_i E_{3\times3} & \boldsymbol{0}_{3\times3} \\ M_i \tilde{c}_i & I_i \end{array} \right] \left[\begin{array}{c} a_i - g \\ \ddot{\theta}_i \end{array} \right] + \left[\begin{array}{c} \boldsymbol{0}_{3\times1} \\ \dot{\theta}_i \times I_i \dot{\theta}_i \end{array} \right] \quad 0 \le f_m \le f_{max_m}, m=1,\ldots,163 \tag{3}$$

where f_m is the muscle force of muscle element m ($m=1,\ldots,163$) and f_{max_m} is the maximum muscle force of muscle element m, i is the segment number (numbering from distal to proximal), L is the number of the proximal muscle element at the segment i, K is the number of the distal muscle element at the segment i, $\boldsymbol{n}_i$ the line of action of the proximal muscle element, $\boldsymbol{n}_{i-1}$ the line of action of the distal muscle element, r_i the moment arm of the proximal muscle element, r_{i-1} the moment arm of the distal muscle element, $\boldsymbol{J}_i$ the proximal joint reaction force, $\boldsymbol{J}_{i-1}$ the distal joint reaction force, I_i the inertia tensor, $\ddot{\theta}_i$ the angular acceleration about COM, $\dot{\theta}_i$ the angular velocity about the COM, a_i the linear acceleration of COM, g the gravitational acceleration, M_i the segment mass, $E_{3\times3}$ the identity matrix, c_i the vector from the proximal joint to the segment COM and d_i is the vector from the proximal to the distal joint, $\tilde{c}_i$ and $\tilde{d}_i$ are the skew sysmetirc matrix of c_i and d_i, respectively.

For each individual subject, eleven lower limb musculoskeletal models were created: one using the subject-specific MR-based dataset and the others through linear scaling of the generic and the remaining nine MR-based datasets. In the scaled models, scaling factors were the ratios of the intersegmental length and width measured of the subject to intersegmental length and width in the underlying dataset. The following anatomical parameters scaled using this methodology were: lines-of-action of muscles/ligament, muscle wrapping parameters, joint centres and contact points [39]. Segment inertia parameters were determined based on the subject's height, mass and gender, using the regression equations in De Leva [44], which were identical in the eleven models. Maximum muscle force of each muscle element was calculated as the maximum muscle stress (60 N/cm^2) [9] multiplied by the PCSA of each muscle element. In total, 330 simulations (10 subjects $\times$ 11 anatomical datasets $\times$ 3 gait trials) were analysed in the study.

D Data analysis and statistics

Predicted muscle force, muscle activation and joint reaction force from models were expressed at a gait cycle percentage from 0% (right heel strike) to 100% (the consecutive right heel strike) at 1% intervals and averaged over three trials. The subject-specific (reference) model was evaluated: first, as a verification of the model the predicted muscle activation was compared to the experimental EMG of this subject. The magnitude (M),

phase (*P*) and combined (*C*) errors were quantified using the Sprague and Geers metric [45], where a combined error of less than 0.40 is the best validation for similar work in the literature [28]; secondly, the predicted knee and hip joint reaction force was compared to the measured data in the literature [46], [47]. The measured knee joint reaction force was from eight subjects with instrumented knee implants [46]; the measured hip joint reaction force was from ten subjects with instrumented hip implants [47].

Differences between the scaled and subject-specific model outputs were quantified using the root mean square difference (RMSD) and normalised by the mean force from the subject-specific model (3):

$$\text{RMSD}_d = \sqrt{\frac{\sum_{i=0}^{100}(F_s^i - F_d^i)^2}{100}}/\overline{F}_s \times 100\ (\%) \tag{4}$$

where F_s is the predicted force from the subject-specific model; F_d is the predicted force using the *d*th scaled model; and $\overline{F}_s$ is the mean force during gait from the subject-specific model.

Pearson correlation and multiple linear regression analyses were used to identify the model in the atlas that produced the closest joint reaction forces to the ones from a subject-specific model. The following anthropometric measurements were investigated: height, mass, body mass index (BMI), limb length, pelvis width, femur length, tibia length, and the limb length to pelvis width ratio. Multiple regressions to the discrepancies in joint reaction forces were identified based on stepwise forward regression ($p_{in} = 0.05$, $p_{out} = 0.1$). The appropriateness of the final regression was checked by inspecting the normal probability plot of the regression standardised residual and the scatterplot of the standardised residual.

A Wilcoxon Signed Rank test was performed to test the hypothesis that scaling of the model (the ten remaining underlying datasets in the atlas) with gender and anthropometric similarity as identified by the regression, produced minor discrepancies of joint reaction force predictions from the subject-specific model, than scaling of a single generic model. The appropriate use of the atlas was tested through the gait data in the "6th Grand Challenge Competition to Predict In Vivo Knee Loads" from one subject (DM, male, height: 172 cm, mass: 70 kg) [48]. The subject-specific model of DM from Ding et al. [39] was implemented in Freebody V2.1 and is freely available at http://www.msksoftware.org.uk/software/freebody. All statistical procedures were performed using IBM SPSS with an alpha level of 0.05 (Version 24.0, IBM Corp., USA).

III Results

Subject-specific modelling of muscle activation showed consistency with the EMG signals (Fig. 2 for a representative subject and see supplementary Fig. A.2 for the other nine subjects). Across all subjects, the quantitative evaluation of predicted muscle activations to EMG data using Sprague and Geers metric is shown in TABLE IV, with phase errors ranging from 0.17 (soleus, standard deviation, SD = 0.06) to 0.32 (rectus femoris, SD = 0.03) and combined errors ranging from 0.26 (soleus, SD = 0.09) to 0.44 (rectus femoris, SD = 0.12)

from the subject-specific models. The predicted muscle activations from ten scaled models to each subject are shown in Supplementary Fig. A.3 with quantitative magnitude (M), phase (P) and combined (C) errors expressed as mean ± standard deviation [range]. When compared to the errors from the subject-specific model, the mean phase errors from the scaled models were greater (p 0.013) for gluteus medius, vastus lateralis, vastus medialis, semitendinosus, soleus and tibialis anterior.

Joint reaction forces predicted from the subject-specific models are shown in Fig. 3 while mean and maximum values from each subject-specific model are summarised in Supplementary TABLE A.I. When compared to the measured forces in the literature, differences in mean and maximum joint reaction forces are 23% and 26% at the knee, 33% and 47% at the hip.

The maximum RMSDs, expressed as the percentage of mean force from the subject-specific model, are shown in Fig. 4. Differences are greater for the muscle forces than the joint forces: in the ankle planar flexors, maximum RMSDs were found to be 336% at flexor hallucis longus and 271% at flexor digitorum longus; in the ankle dorsiflexors, 325% and 301% at tibialis anterior and extensor digitorum longus, respectively; in the knee extensors 465% at vastus lateralis; and in the hip adductors, 448% at gracilis. The differences in joint reaction forces were greatest at the knee joint with a maximum RMSD of 61%, followed by the ankle joint with 48% and hip joint with 30%. The maximum RMSD of the sum of joint reaction forces (ankle, knee and hip) was 26% from the scaled model, in comparison with the sum of these from the subject-specific model.

A significant moderate to strong correlation ($R > 0.30$, $p < 0.05$) was found between the discrepancies in the joint reaction force predictions and the discrepancies in gender and anthropometric measurements of the underlying anatomical datasets (apart from the pelvis width, see TABLE V).

The final multiple regression found the significant predictors to the difference in the joint reaction force predictions, which are, for the different predictions of the ankle joint forces: the differences in gender (regression coefficient, $B = 7.66$, $p = 0.005$) and mass ($B = 0.49$, $p < 0.001$); for the different predictions of knee joint forces: differences in gender ($B = 7.75$, $p = 0.013$), mass ($B = 0.38$, $p = 0.001$), limb length ($B = 1.00$, $p = 0.017$), and the limb length to pelvis width ratio ($B = 37.22$, $p = 0.011$); for the different predictions of hip joint forces: differences in gender ($B = 2.64$, $p = 0.039$), mass ($B = 0.10$, $p = 0.033$) and limb length ($B = 0.38$, $p < 0.001$); and for the different predictions of the sum of these: differences in gender ($B = 25.24$, $p = 0.003$), mass ($B = 0.99$, $p = 0.001$) and limb length ($B = 2.23$, $p = 0.046$) (Fig. 5 and TABLE VI). The regression models accounted for 49%, 61%, 36% and 40% of the variances of the differences at the ankle, knee, hip joint force predictions, and the sum of these, respectively (TABLE VI).

In comparison with the RMSDs produced by scaling of the generic model, scaling of the musculoskeletal model with gender and anthropometric similarity as identified by the regression significantly reduced the RMSDs in joint reaction forces of ankle, knee, hip and their sum ($p = 0.005$, TABLE VII).

Based on the regression to the knee joint force prediction, the closest scaled model in the atlas was identified for subject DM in the "6th Grand Challenge Competition to Predict In Vivo Knee Loads". It produced similar values as the subject-specific model for RMSE and R^2 when compared to the measured knee joint reaction force, as shown in Fig. 6 for two representative gait cycles. The RMSE from the closest model was lower than the RMSEs from all other ten models in the atlas.

IV Discussion

Use of a single, scaled generic musculoskeletal model is unable to account for wide inter-individual variability in lower limb anatomy [27] – [29]. This study for the first time has demonstrated that the discrepancies from the scaled models are significantly correlated with the discrepancies in gender and anthropometric measurements of the underlying anatomical datasets when compared to a subject-specific model. The discrepancy in mass was the primary anthropometric predictor of the discrepancy in the ankle joint force prediction and the discrepancy of limb length was the primary anthropometric predictor of the discrepancies in knee and hip joint force predictions. After mass and limb length, the limb length to pelvis width ratio was found to be the third significant predictor: it accounted for an additional 3% of the variance of discrepancies at the knee. Therefore, these anthropometric measures should be taken into account and varied when creating a comprehensive lower limb anatomical atlas.

The differences in predicting the knee and hip joint forces are expected as there are known gender differences in pelvic shape [18], [49] and there is some evidence of gender differences at the distal femur [50]. Such differences are not accounted for by scaling of one unique gender model. These differences may promulgate throughout the whole lower limb force predictions through the action of biarticular muscles [51]. Our study has shown that these gender differences do not dominate differences in joint reaction force predictions, when compared to anthropometry, but do improve the fit of the regression of RMSDs by 5% at the ankle ($p = 0.005$), 3% at the knee ($p = 0.013$), 2% at the hip ($p = 0.039$) and 6% for their sum ($p = 0.009$).

Linear scaling of a dataset with same gender and similar anthropometry to the subject reduced discrepancies when compared to scaling of a generic dataset: discrepancies were reduced at the ankle joint from 44% to 16%, a 64% reduction ($p = 0.005$); at the knee joint from 48% to 16%, a 67% reduction ($p = 0.005$); and at the hip joint from 34% to 17%, a 50% reduction ($p = 0.005$). The reduction was most evident for subjects with lower body mass, for example, subject M5 showed a reduction of 89% at the ankle joint and 77% at the hip joint. As a demonstration of the use of the atlas, scaling of the closest model to one subject in the literature with an instrumented knee implant produced knee joint forces consistent with the measured knee joint forces (R^2 0.78). The RMSE from the scaled closest model was comparable to the best ones that can be obtained from the subject-specific model. The results support our hypothesis. It is worth noting that the subject-specific model of DM predicted lower later-stance knee forces than the scaled closest model. This may be attributed the geometry differences between the artificial knee and the natural knee [52], [53]. Previous studies have found that muscle architecture scales with subject morphology,

such as body mass and limb length [11]. The results of our study, however, suggest that the muscle attachments may not scale with these morphological parameters, highlighting the importance of having an anatomical atlas that far closer represents the subjects.

There are methodological differences between the generic and MR-based datasets which may affect the consistency of the atlas. First, joint centres and axes were measured using the functional method in [12] and measured based on joint geometry from the MR images. Additionally, the foot was maintained in plantar flexion position during the cadaveric measurement [12] and was in a more neutral position in the MR scanners. The MRI-based anatomical datasets showed a good consistency as indicated by the high coefficient of determination value of over 0.96 in joint reaction forces (TABLE VII).

Scaling using the closest anatomical model still produced a discrepancy of 16% in joint reaction force predictions, when compared to the subject-specific model. This discrepancy corresponds to a 0.37 BW difference for hip joint force during gait. In addition, the final regression model for the hip joint only accounted for approximately 33% of variance (adjusted $R^2 = 0.333$) of the discrepancy. This indicates that the linear scaling based on the gender and anthropometric similarity may not be adequate, especially for the hip joint force prediction. Recent studies have demonstrated a better estimation of muscle attachment sites by applying a morphing technique to the bone surface when compared to linear scaling [54], [55]. This technique could in future be applied to generate a larger, population-based dataset of subject-specific musculoskeletal models.

To facilitate the development of subject-specific musculoskeletal models, the entire anatomical atlas is accessible at http://www.msksoftware.org.uk, including segmented bone surfaces (STL files), bony landmark coordinates, joint centres, contact points, lines-of-action of muscles and ligaments, wrapping object parameters and muscle parameters. Subject-specific musculoskeletal models from the atlas implemented in FreeBody are available in the same repository. The fidelity of subject-specific musculoskeletal models was evaluated by comparing the predicted muscle activation against the experimental EMG of the same subject, and secondly, by comparing the calculated joint reaction forces against the instrumented implant measurements from other subjects in the literature. EMG patterns from eight muscles were comparable with the literature [56], [57] and the errors between muscle activations and EMG were comparable with other validation studies [28], [39]. Considerable differences were found between the higher calculated joint reaction forces with the measured joint reaction forces in the literature. This can be partially explained by the discrepancy between the artificial joint and the natural joint and subsequently, the discrepancy introduced in gait: a slightly higher walking speed and greater ground reaction force were found from our young healthy subjects and so a higher joint reaction force is expected. We acknowledge that improvements to the musculoskeletal geometry alone may not be sufficient to minimise the disagreement between model outcomes and true physiological loading in the musculoskeletal system. Other improvements in the literature focusing on taking greater account of realistic neuromuscular strategies have enabled better estimation of muscle activation and joint reaction force. These improvements include EMG-driven musculoskeletal models [58] – [60] and subject-specific synergy controls [61], [62].

There are some limitations to this study. First the muscle parameters including fibre length to muscle length ratio ($\frac{L_f}{L_m}$), pennation angle (θ), and sarcomere length (L_s) were obtained from studies of elderly cadavers [10], [12]. Until now, there is no complete and comprehensive dataset measuring these parameters in vivo and it is known that uncertainty in these parameters can affect muscle force predictions significantly [63], [64]; they cannot be obtained from MRI. Second, MR images were acquired in the standardised position of subjects lying in the MR scanner, resulting in a muscle moment arm definition for that position only; the variation in muscle moment arm during dynamic and loaded conditions was not taken into account. Some studies have recently demonstrated the feasibility for physiological measurements of muscle moment arms over a range of joint motion [65], [66] and using this approach will provide a better representation of the musculoskeletal geometry during functional activities. Third, in our optimisation model, each muscle element was modelled with a constant strength and it was independent of any contraction dynamics associated with muscle length and velocity. For muscles that covered a large muscle attachment site, their strength was evenly distributed across the separate elements and the effect of this muscle decomposition was not corrected in the cost function in either the subject-specific model or the scaled model. Decomposition and muscle dynamics have been shown to affect the prediction of muscle forces [28], [67]. Finally, the errors quantified in the study were from healthy subjects during gait only and thus the effect of extrapolating these results to other activities and pathological subject should be investigated.

V   Conclusion

This study tested the hypothesis that linear scaling to a musculoskeletal model with gender and anthropometric similarity to the individual subject can produce similar results to the ones that can be obtained from a subject-specific model. A lower limb musculoskeletal anatomical atlas, consisting of datasets derived from MRI and a generic dataset from the literature, was developed; the discrepancies from scaled models were quantified where joint reaction forces from the personalised, subject-specific musculoskeletal models are considered as references; and finally, the use of the atlas was identified based on gender and anthropometric similarity. This method produced the lowest discrepancies when compared to the other linearly scaled models, thus supporting our hypothesis. Discrepancies of 16% in joint reaction force calculations remain, indicating that there is potential for further improvements. We have provided a new anatomical atlas that is publically available to accelerate the development and adoption of subject-specific musculoskeletal models.

Supplementary Material

Refer to Web version on PubMed Central for supplementary material.

Acknowledgments

References

[1]. Farris DJ, et al. Musculoskeletal modelling deconstructs the paradoxical effects of elastic ankle exoskeletons on plantar-flexor mechanics and energetics during hopping. J Exp Biol. 2014 Nov.15:4018–4028.

[2]. Rane L, Bull AMJ. Functional electrical stimulation of gluteus medius reduces the medial joint reaction force of the knee during level walking. Arthritis Res Ther. 2016 Nov; 18(1):255–266. [PubMed: 27809923]

[3]. Hincapie JG, et al. Musculoskeletal model-guided, customizable selection of shoulder and elbow muscles for a C5 SCI neuroprosthesis. IEEE Trans Neural Syst Rehabil Eng. 2008 Jun; 16(3):255–263. [PubMed: 18586604]

[4]. Silverman AK, Neptune RR. Three-dimensional knee joint contact forces during walking in unilateral transtibial amputees. J Biomech. 2014 Aug; 47(11):2556–2562. [PubMed: 24972921]

[5]. Heller MO, et al. Influence of prosthesis design and implantation technique on implant stresses after cementless revision THR. J Orthop Surg Res. 2011 May; 6(1):1–9. [PubMed: 21208449]

[6]. Pandis P, Prinold JAI, Bull AMJ. Shoulder muscle forces during driving: Sudden steering can load the rotator cuff beyond its repair limit. Clin Biomech. 2015 Oct; 30(8):839–846.

[7]. Delp SL, et al. An interactive graphics-based model of the lower extremity to study orthopaedic surgical procedures. IEEE Trans Biomed Eng. 1990 Aug; 37(8):757–67. [PubMed: 2210784]

[8]. Arnold EM, et al. A model of the lower limb for analysis of human movement. Ann Biomed Eng. 2010 Feb; 38(2):269–279. [PubMed: 19957039]

[9]. Rajagopal A, et al. Full body musculoskeletal model for muscle-driven simulation of human gait. IEEE Trans Biomed Eng. 2016 Oct; 63(10):2068–79. [PubMed: 27392337]

[10]. Ward SR, et al. Are current measurements of lower extremity muscle architecture accurate? Clin Orthop Relat Res. 2009 Apr; 467(4):1074–1082. [PubMed: 18972175]

[11]. Handsfield GG, et al. Relationships of 35 lower limb muscles to height and body mass quantified using MRI. J Biomech. 2014 Feb; 47(3):631–638. [PubMed: 24368144]

[12]. Klein Horsman MD, et al. Morphological muscle and joint parameters for musculoskeletal modelling of the lower extremity. Clin Biomech. 2007 Feb; 22(2):239–247.

[13]. Carbone V, et al. TLEM 2.0 – a comprehensive musculoskeletal geometry dataset for subject-specific modeling of lower extremity. J Biomech. 2015 Mar; 48(5):1–8. [PubMed: 25435385]

[14]. Cleather DJ, Bull AMJ. The development of lower limb musculoskeletal models with clinical relevance is dependent upon the fidelity of the mathematical description of the lower limb. Part 2: patient-specific geometry. Proc Inst Mech Eng Part H J Eng Med. 2012; 226(2):133–145.

[15]. Mossenet F, Chèze L, Dumas R. Influence of the level of muscular redundancy on the validity of a musculoskeletal model. J Biomech Eng. 2016 Feb; 138(2):1–6.

[16]. Correa TA, et al. Accuracy of generic musculoskeletal models in predicting the functional roles of muscles in human gait. J Biomech. 2011 Jul; 44(11):2096–2105. [PubMed: 21703627]

[17]. Andersen MS, et al. A computationally efficient optimisation-based method for parameter identification of kinematically determinate and over-determinate biomechanical systems. Comput Methods Biomech Biomed Engin. 2010; 13(2):171–83. [PubMed: 19693717]

[18]. Kepple TM, et al. A three-dimensional musculoskeletal database for the lower extremities. J Biomech. 1998 Jan; 31(1):77–80. [PubMed: 9596541]

[19]. Duda GN, et al. Variability of femoral muscle attachments. J Biomech. 1996 Sep; 29(9):1185–1190. [PubMed: 8872275]

[20]. Bosmans L, et al. Sensitivity of predicted muscle forces during gait to anatomical variability in musculotendon geometry. J Biomech. 2015 Jul; 48(10):2116–2123. [PubMed: 25979383]

[21]. Scheys L, et al. Personalized MR-based musculoskeletal models compared to rescaled generic models in the presence of increased femoral anteversion: effect on hip moment arm lengths. Gait Posture. 2008 Oct; 28(3):358–365. [PubMed: 18571416]

[22]. Zhang KY, et al. The relationship between lateral meniscus shape and joint contact parameters in the knee: a study using data from the osteoarthritis initiative. Arthritis Res Ther. 2014 Jan.16(1):R27. [PubMed: 24467794]

[23]. Prinold JAI, et al. A patient-specific foot model for the estimate of ankle joint forces in patients with juvenile idiopathic arthritis. Ann Biomed Eng. 2016 Jan; 44(1):247–257. [PubMed: 26374518]

[24]. Smith DK, et al. Validation of three-dimensional reconstructions of knee anatomy: CT vs MR imaging. J Comput Assist Tomogr. 1989; 13(2):294–301. [PubMed: 2925917]

[25]. Arnold AS, et al. Accuracy of muscle moment arms estimated from MRI-based musculoskeletal models of the lower extremity. Comput Aided Surg. 2000; 5:108–119. [PubMed: 10862133]

[26]. Lerner ZF, et al. How tibiofemoral alignment and contact locations affect predictions of medial and lateral tibiofemoral contact forces. J Biomech. 2015 Jan; 48(4):644–650. [PubMed: 25595425]

[27]. Gerus P, et al. Subject-specific knee joint geometry improves predictions of medial tibiofemoral contact forces. J Biomech. 2013 Sep; 46(16):2778–2786. [PubMed: 24074941]

[28]. Marra MA, et al. A subject-specific musculoskeletal modeling framework to predict in vivo mechanics of total knee arthroplasty. J Biomech Eng. 2014 Feb.137(2)

[29]. Jung Y, Phan CB, Koo S. Intra-articular knee contact force estimation during walking using force-reaction elements and subject-specific joint model. J Biomech Eng. 2016 Feb.138(2)

[30]. Bolsterlee B, Veeger DHEJ, Chadwick EK. Clinical applications of musculoskeletal modelling for the shoulder and upper limb. Med Biol Eng Comput. 2013 Sep; 51(9):953–963. [PubMed: 23873010]

[31]. Pheasant, S, Haslegrave, CM. Bodyspace: Anthropometry, Ergonomics, and the Design of Work. London: Taylor and Francis; 2006. 244

[32]. Wu G, et al. ISB recommendation on definitions of joint coordinate system of various joints for the reporting of human joint motion--part I: ankle, hip, and spine. International Society of Biomechanics. J Biomech. 2002 Apr.35:543–548. [PubMed: 11934426]

[33]. Lieber RL, Loren GJ, Friden J. In vivo measurement of human wrist extensor muscle sarcomere length changes. J Neurophysiol. 1994 Mar; 71(3):874–881. [PubMed: 8201427]

[34]. Duffell LD, Hope N, McGregor AH. Comparison of kinematic and kinetic parameters calculated using a cluster-based model and Vicon's plug-in gait. Proc Inst Mech Eng H. 2014 Feb; 228(2):206–10. [PubMed: 24449800]

[35]. Greenwood NL, et al. Electromyographic activity of pelvic and lower limb muscles during postural tasks in people with benign joint hypermobility syndrome and non hypermobile people. A pilot study. Man Ther. 2011 Aug; 16(6):623–628. [PubMed: 21831693]

[36]. Zipp P. Recommendations for the standardization of lead positions in surface electromyography. Eur J Appl Physiol Occup Physiol. 1982; 50(1):41–54.

[37]. Arnold EM, et al. How muscle fiber lengths and velocities affect muscle force generation as humans walk and run at different speeds. J Exp Biol. 2013 Jun.216:2150–2160. [PubMed: 23470656]

[38]. Cleather DJ, Bull AMJ. The development of a musculoskeletal model of the lower limb: introducing FREEBODY. R Soc Open Sci. 2015 Jun.2(6)

[39]. Ding Z, et al. In vivo knee contact force prediction using patient-specific musculoskeletal geometry in a segment-based computational model. J Biomech Eng. 2016 Feb.138(2)

[40]. Horn BKP. Closed form solution of absolute orientation using unit quaternions. J Opt Soc Am A. 1987 Apr.4:629–642.

[41]. Dumas R, Aissaoui R, de Guise JA. A 3D generic inverse dynamic method using wrench notation and quaternion algebra. Comput Methods Biomech Biomed Engin. 2004 Jun; 7(3):159–166. [PubMed: 15512759]

[42]. Cleather DJ, Goodwin JE, Bull AMJ. An optimization approach to inverse dynamics provides insight as to the function of the biarticular muscles during vertical jumping. Ann Biomed Eng. 2011 Jan; 39(1):147–160. [PubMed: 20862546]

[43]. Crowninshield RD, Brand RA. A physiologically based criterion of muscle force prediction in locomotion. J Biomech. 1981; 14(11):793–801. [PubMed: 7334039]

[44]. De Leva P. Adjustments to zatsiorsky-seluyanov's segment inertia parameters. J Biomech. 1996; 29(9):1223–1230. [PubMed: 8872282]

[45]. Schwer LE. Validation metrics for response histories: perspectives and case studies. Eng Comput. 2007 Dec; 23(4):295–309.

[46]. Bergmann G, et al. Standardized loads acting in knee implants. PLoS One. 2014 Jan.9(1)

[47]. Bergmann G, et al. Standardized loads acting in hip implants. PLoS One. 2016 May.11(5)

[48]. Fregly BJ, et al. Grand challenge competition to predict in vivo knee loads. J Orthop Res. 2012 Apr; 30(4):503–513. [PubMed: 22161745]

[49]. Nakahara I, et al. Gender differences in 3D morphology and bony impingement of human hips. J Orthop Res. 2011 Mar; 29(3):333–339. [PubMed: 20939047]

[50]. Griffin FM, et al. Anatomy of the epicondyles of the distal femur: MRI analysis of normal knees. J Arthroplasty. 2000 Apr; 15(3):354–359. [PubMed: 10794232]

[51]. Cleather DJ, Goodwin JE, Bull AMJ. An optimization approach to inverse dynamics provides insight as to the function of the biarticular muscles during vertical jumping. Ann Biomed Eng. 2011 Jan; 39(1):147–160. [PubMed: 20862546]

[52]. Zhao D, et al. In vivo medial and lateral tibial loads during dynamic and high flexion activities. J Orthop Res. 2007 Feb; 25(5):593–602. [PubMed: 17290383]

[53]. Saliba CM, Brandon SCE, Deluzio KJ. Sensitivity of medial and lateral knee contact force predictions to frontal plane alignment and contact locations. J Biomech. 2017 May.57:125–130. [PubMed: 28342531]

[54]. Nolte D, et al. Non-linear scaling of a musculoskeletal model of the lower limb using statistical shape models. J Biomech. 2016 Oct; 49(14):3576–3581. [PubMed: 27653375]

[55]. Pellikaan P, et al. Evaluation of a morphing based method to estimate muscle attachment sites of the lower extremity. J Biomech. 2014 Mar; 47(5):1144–1150. [PubMed: 24418197]

[56]. Cappellini G, Ivanenko Y. Motor patterns in human walking and running. J Neurophysiol. 2006 Jun; 95(6):3426–3437. [PubMed: 16554517]

[57]. Hamner SR, Seth A, Delp SL. Muscle contributions to propulsion and support during running. J Biomech. 2010 Oct; 43(14):2709–2716. [PubMed: 20691972]

[58]. Hoang HX, et al. Subject-specific calibration of neuromuscular parameters enables neuromusculoskeletal models to estimate physiologically plausible hip joint contact forces in healthy adults. J Biomech. 2018 Aug.80:111–120. [PubMed: 30213647]

[59]. Pizzolato C, et al. CEINMS: A toolbox to investigate the influence of different neural control solutions on the prediction of muscle excitation and joint moments during dynamic motor tasks. J Biomech. 2015 Nov; 48(14):3929–3936. [PubMed: 26522621]

[60]. Durandau G, Farina D, Sartori M. Robust real-time musculoskeletal modelling driven by electromyograms. IEEE Trans Biomed Eng. 2018 Mar; 65(3):556–564. [PubMed: 28504931]

[61]. Walter JP, et al. Muscle synergies may improve optimization prediction of knee contact forces during walking. J Biomech Eng. 2014 Feb.136(2)

[62]. Serrancolí G, et al. Neuromusculoskeletal model calibration significantly affects predicted knee contact forces for walking. J Biomech Eng. 2016 Aug; 138(8):1–11.

[63]. Redl C, Gfoehler M, Pandy MG. Sensitivity of muscle force estimates to variations in muscle – tendon properties. J Biomech. 2007 Apr.26:306–319.

[64]. Carbone V, et al. Sensitivity of subject-specific models to Hill muscle – tendon model parameters in simulations of gait. J Biomech. 2016 Jun; 49(9):1953–1960. [PubMed: 27131851]

[65]. Blemker SS, et al. Image-based musculoskeletal modeling: applications, advances, and future opportunities. J Magn Reson Imaging. 2007 Feb.451:441–451.

[66]. Tsai LC, Colletti PM, Powers CM. Magnetic resonance imaging-measured muscle parameters improved knee moment prediction of an EMG-driven model. Med Sci Sports Exerc. 2012 Feb; 44(2):305–312. [PubMed: 21775905]

[67]. Holmberg LJ, Klarbring A. Muscle decomposition and recruitment criteria influence muscle force estimates. Multibody Syst Dyn. 2012 Sep; 28(3):283–289.
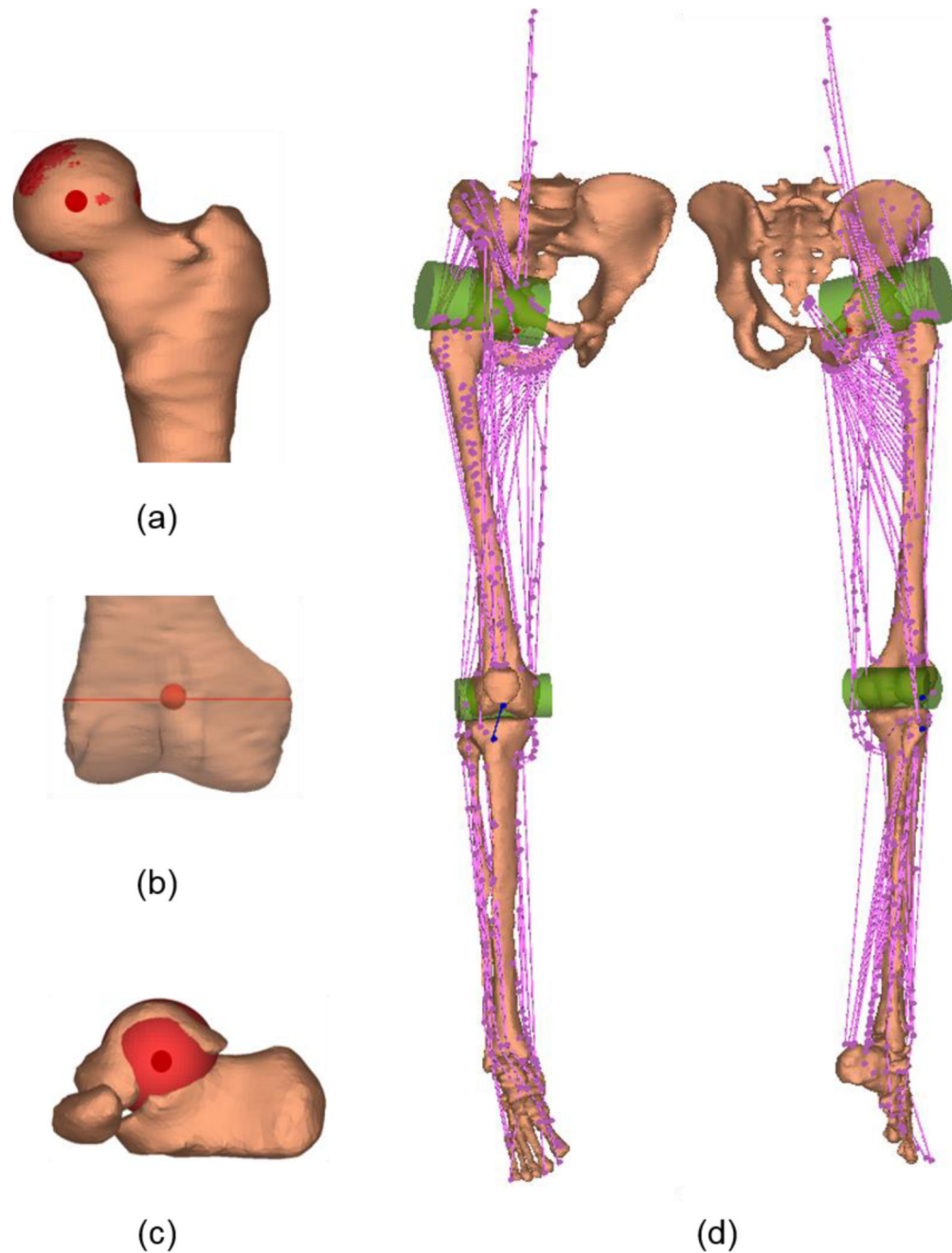
Fig. 1.
Lower limb anatomy geometry for a representative subject. (a) Hip centre (b) Knee centre and knee axis (c) Ankle centre; (d) Muscle element lines-of-action (in pink) and patella ligament (in blue). Wrapping objects (in green) were defined for iliopsoas and gastrocnemius.
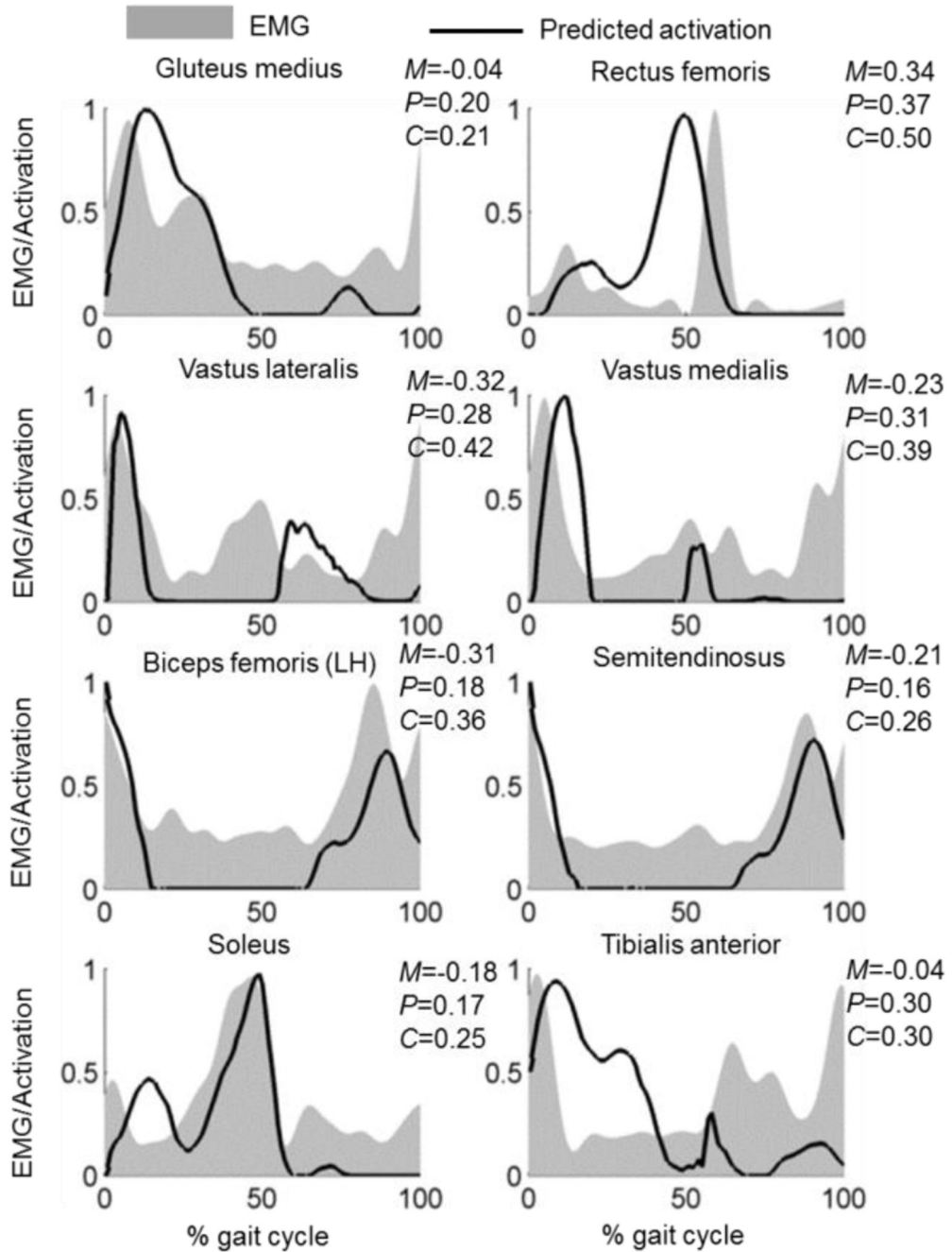
Fig. 2.
Predicted muscle activations (solid line) from the subject-specific model compared to the experimental EMG data (grey area) in a representative subject (F1). EMG data were individually normalised to the maximum recorded signal of each muscle during gait and predicted muscle activations were defined to be between 0 (fully deactivated) and 1 (fully activated) in terms of the peak value predicted during gait. Magnitude (M), phase (P) and combined (C) errors from predicted muscle activations are quantified using Sprague and Geers metric. See supplementary Fig. A.2 for the results of the other nine subjects.
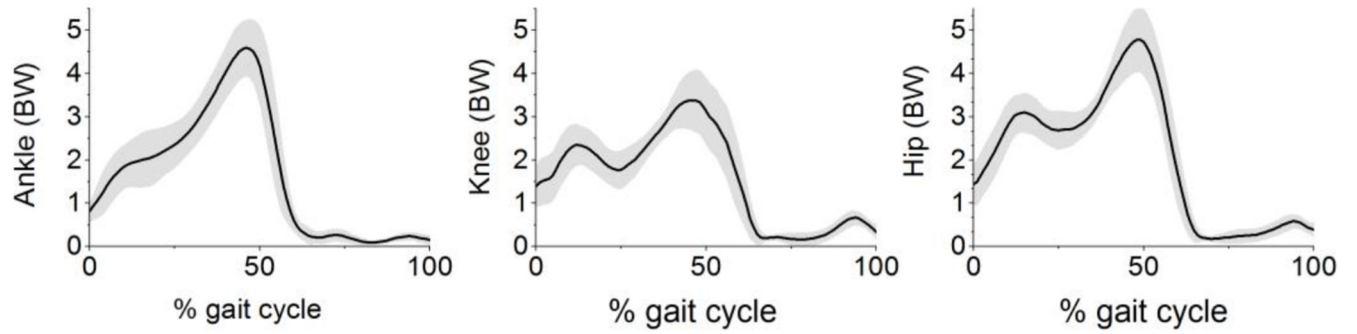
Fig. 3.
Mean joint reaction force (solid line) and standard deviation (shaded area), expressed in bodyweight (BW), from ten subject-specific models at the ankle, knee and hip joint. Mean and maximum joint reaction force for each subject-specific model is reported in Supplementary TABLE A.I.
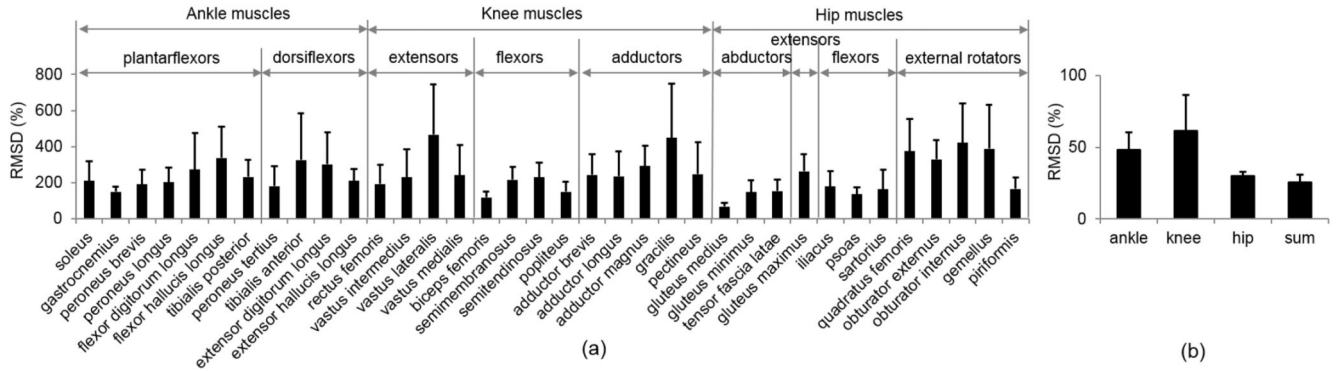
Fig. 4.
RMSDs in muscle and joint reaction forces: (a) maximum RMSDs and standard deviations in muscle forces crossing the ankle, knee and hip joints, (b) maximum RMSDs and standard deviations in ankle, knee and hip joints, and the sum of these. RMSDs are expressed as a percentage of mean force from the subject-specific model.
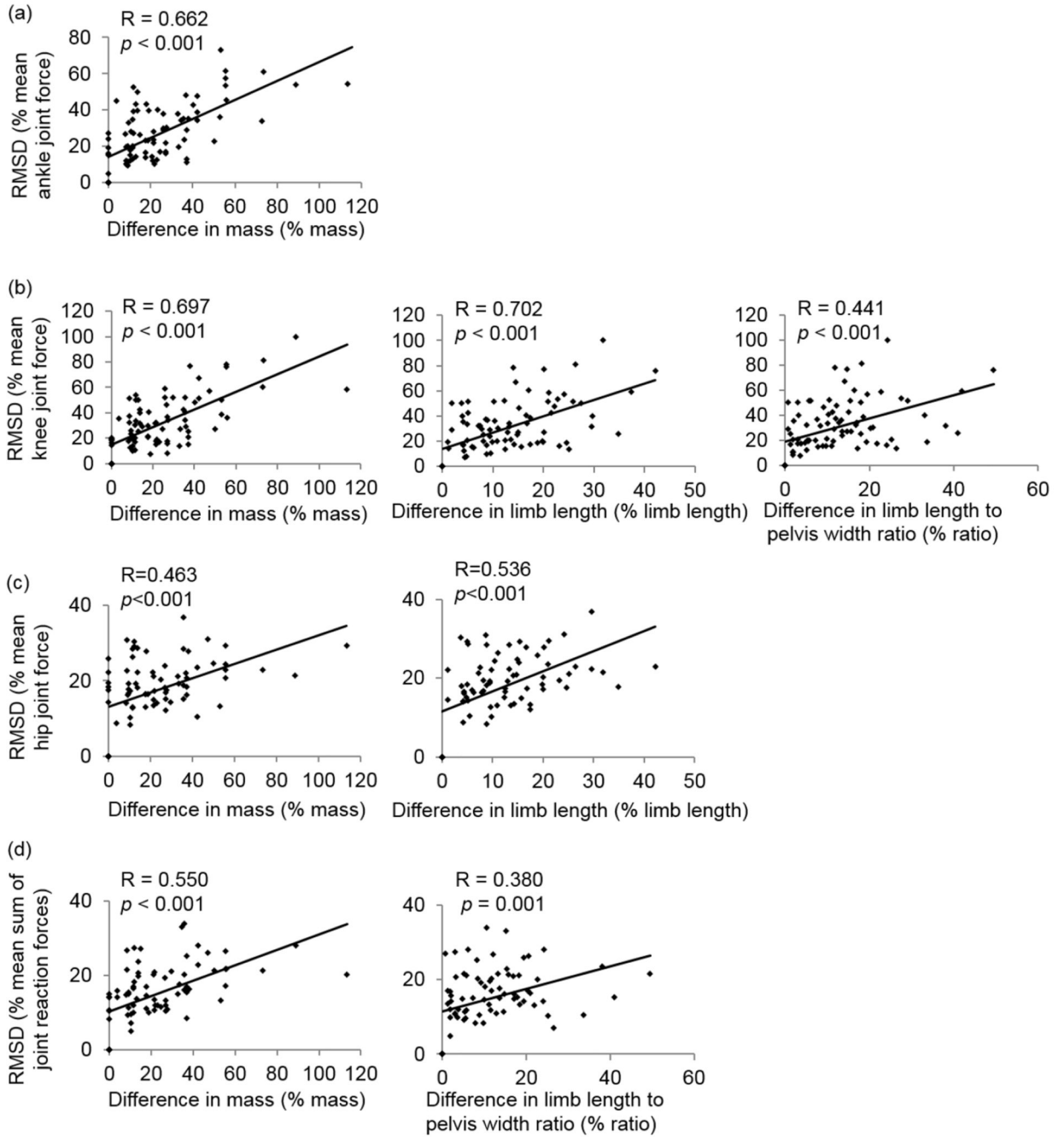
Fig. 5.
Significant anthropometric predictors of root mean square difference (RMSD) in joint forces at (a) the ankle, (b) the knee, (c) the hip and (d) the sum of all joints. Difference in anthropometric measurements is expressed as a percentage difference from the underlying dataset to the subject. R and *p* values are from the Pearson correlation analysis.
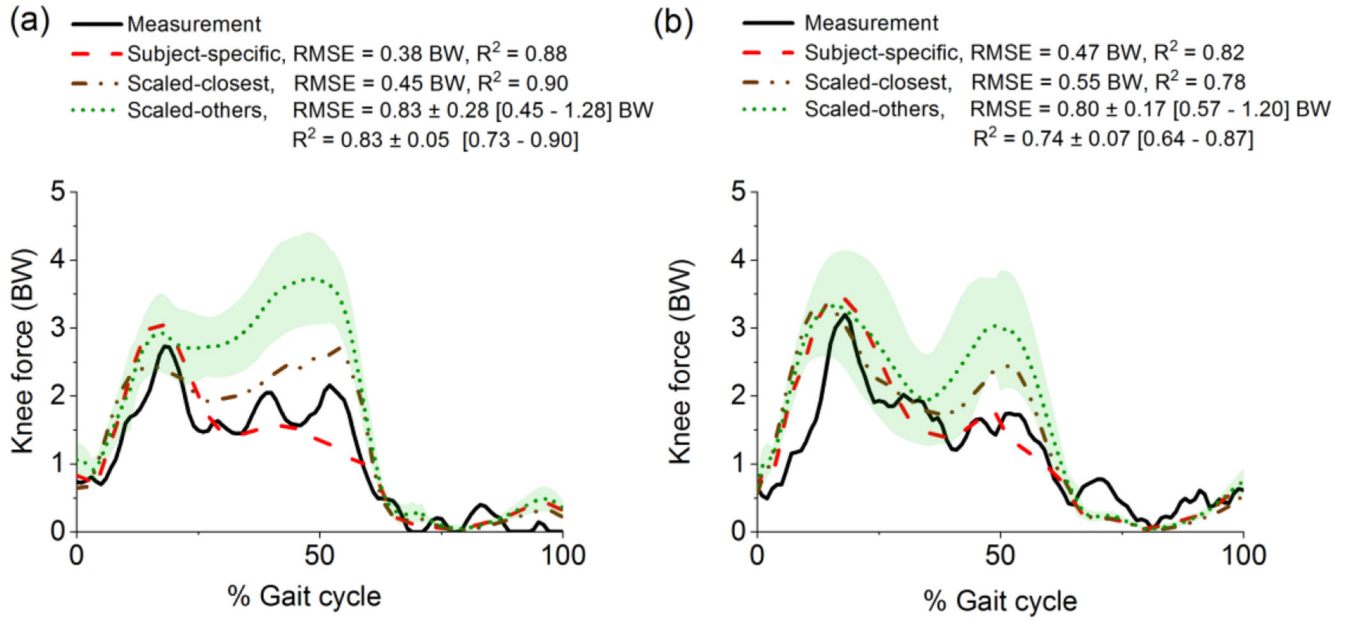
Fig. 6.

Predicted knee joint reaction force, expressed in body weight (BW), using eleven models in the atlas compared to the experimental measurement (solid line) and the subject-specific prediction (dashed line) in two representative gait cycles: (a) DM_ngait1 and (b) DM_bouncy5. The subject-specific model of DM from Ding et al. [39] is freely available at http://www.msksoftware.org.uk/software/freebody. The scaled-closest model is identified based on the regression; the scaled-others are presented as mean (dotted line) and standard deviations (shaded area). The root mean square error (RMSE) and coefficient of determination (R^2) are calculated by comparing the difference between the model prediction with the experimental measurement. The RMSE and R^2 from the scaled-others models are expressed as mean ± standard deviation [range].

Table I

Single Complete Subject Lower Limb Musculoskeletal Generic Models Used in the Literature

Model	Gender	Height (m)	Body mass (kg)	Lower limb length (mm)	Age (years)
Rajagopal et al.[9]	Male	1.70	75	not provided	not provided
Carbone et al.[13]	Male	not provided	45	813	85
Klein Horsman et al.[12]	Male	1.74	105	904[a]	77

[a]Limb length is calculated as the sum of femur and tibia lengths of the right leg: femur length is measured as the distance from the trochanter major to the mid point of the femoral epicondyles; tibia length is measured as the distance from the mid point of the femoral epicondyles to the medial malleolus.

Table II

Participant Characteristics

Subject	Age (years)	Height (m)	Height percentile (%ile)[a]	Body mass (kg)	Limb length (mm)[b]
Male 1	27	1.92	99th	85.0	910
Male 2	42	1.83	90th	96.0	836
Male 3	25	1.80	80th	70.0	876
Male 4	28	1.72	39th	70.0	787
Male 5	21	1.68	20th	64.0	727
Female 1	43	1.84	99th	78.0	873
Female 2	45	1.68	87th	70.0	796
Female 3	39	1.64	68th	61.6	757
Female 4	24	1.58	31th	55.6	714
Female 5	27	1.55	17th	45.0	690
Mean (SD)	32 (9)	1.72 (0.12)		69.5 (14.5)	797 (76)

[a] Height percentile is calculated based on British adults [31].

[b] Limb length is calculated as the sum of femur and tibia lengths of the right leg: femur length is measured as the distance from the major trochanter to the mid point of the femoral epicondyles; tibia length is measured as the distance from the mid point of the femoral epicondyles to the medial malleolus.

Table III
Muscle Parameters of a Representative Subject (F1)

Muscle	PCSA (cm²)	Muscle volume (V_m, cm³)	Muscle length (L_m, cm)	Fibre length to muscle length ratio ($\frac{L_f}{L_m}$)	Pennation angle (θ, °)	sarcomere length (L_s, μm)
Adductor brevis	11.26	118.05	14.23	0.68	6.10	2.91
Adductor longus	14.79	181.49	21.91	0.50	7.10	3.00
Adductor magnus	58.58	631.19	32.82	0.39	15.50	2.19
Biceps femoris long head	31.75	234.49	29.68	0.28	11.60	2.35
Biceps femoris short head	6.80	112.43	26.89	0.49	12.30	3.31
Extensor digitorum longus [a]	7.28	77.90	37.89	0.24	10.80	3.12
Extensor hallucis longus [a]	2.64	37.74	37.89	0.31	9.40	3.24
Flexor digitorum longus	8.50	34.53	26.02	0.16	13.60	2.56
Flexor hallucis longus	19.87	87.53	24.01	0.20	16.90	2.37
Gastrocnemius lateral	24.32	169.44	25.14	0.27	12.00	2.71
Gastrocnemius medial	55.89	290.70	28.11	0.19	9.90	2.59
Gemellus inferior [b]	1.01	7.29	7.20	1.00	0.00	2.70
Gemellus superior [b]	1.01	7.29	7.20	1.00	0.00	2.70
Gluteus maximus	49.01	958.03	30.38	0.62	21.90	2.60
Gluteus medius	51.94	364.58	19.99	0.37	20.50	2.40
Gluteus minimus	8.78	118.05	13.44	1.00	0.00	2.70
Gracilis	3.63	117.24	33.70	0.79	8.20	3.24
Iliacus	11.76	199.15	26.19	0.56	14.30	3.02
Obturator externus	5.92	61.03	10.30	1.00	0.00	2.70
Obturator internus	3.68	30.52	8.29	1.00	0.00	2.70
Pectineus	5.53	73.88	13.36	1.00	0.00	2.70
Peroneus brevis [c]	6.47	47.38	37.10	0.19	11.50	2.76
Peroneus longus [c]	13.54	99.58	37.10	0.19	14.10	2.72
Peroneus tertius [d]	6.20			1.00	0.00	2.70
Piriformis	4.88	48.99	10.04	1.00	0.00	2.70
Plantaris [d]	2.40			1.00	0.00	2.70
Popliteus	2.64	26.50	10.04	1.00	0.00	2.70
Psoas minor [d]	1.10			1.00	0.00	2.70
Psoas	15.30	305.16	34.05	0.50	10.60	3.11
Quadratus femoris	4.76	36.14	7.60	1.00	0.00	2.70
Rectus femoris	46.82	304.35	33.52	0.21	13.90	2.42
Sartorius	3.22	183.90	55.00	0.90	1.30	3.11
Semimembranosus	40.63	277.85	28.46	0.24	15.10	2.61
Semitendinosus	9.06	208.79	32.30	0.65	12.90	2.89

Muscle	PCSA (cm^2)	Muscle volume (V_m, cm^3)	Muscle length (L_m, cm)	Fibre length to muscle length ratio ($\frac{L_f}{L_m}$)	Pennation angle (θ, °)	sarcomere length (L_s, μm)
Soleus	151.65	498.69	33.52	0.11	28.30	2.12
Tensor fasciae latae	4.31	71.47	16.59	1.00	0.00	2.70
Tibialis anterior	14.01	153.38	33.09	0.27	9.60	3.14
Tibialis posterior	31.23	119.65	31.95	0.12	13.70	2.56
Vastus intermedius	45.99	308.37	34.66	0.24	4.50	2.17
Vastus lateralis	76.97	936.35	38.32	0.38	18.40	2.14
Vastus medialis	67.23	486.64	34.48	0.22	29.60	2.24

Fibre length to muscle length ratio ($\frac{L_f}{L_m}$), pennation angle (θ), and sarcomere length (L_s) were taken from [10]. For muscles which were not measured in [10] their fibre length to muscle length ratio was set as 1, pennation angle was set as 0° and sarcomere length was set as 2.7μm.

[a] Muscle volume was only available for the combined extensor digitorum longus and extensor hallucis longus in [11]. Volume proportion in [12] was used to divide the two muscles.

[b] Muscle volume was only available for the combined gemellus inferior and gemellus superior in [11]. Volume proportion in [12] was used to divide the two muscles.

[c] Muscle volume was only available for the combined peroneus longus and peroneus brevis in [11]. Volume proportion in [12] was used to divide the two muscle.

[d] Muscle was not included in [11]. Its PCSA was obtained from [12].

Table IV

Absolute Values of Magnitude (*M*), Phase (*P*) and Combined (*C*) Errors Between Predicted Muscle Activations From Models (Subject-Specific and Scaled Models) to Measured EMG Data, Reported as Mean (Standard Deviation) for All Ten Subjects

	M			*P*			*C*		
	Subject-specific model	Scaled model	*p* value[a]	Subject-specific model	Scaled model	*p* value[a]	Subject-specific model	Scaled model	*p* value[a]
Gluteus medius	0.22 (0.13)	0.34 (0.20)	0.028	0.20 (0.03)	0.24 (0.02)	0.013	0.31 (0.10)	0.44 (0.17)	0.017
Rectus femoris	0.26 (0.20)	0.38 (0.24)	0.013	0.32 (0.03)	0.34 (0.04)	0.799	0.44 (0.12)	0.53 (0.18)	0.047
Vastus lateralis	0.20 (0.09)	0.37 (0.09)	0.005	0.27 (0.08)	0.40 (0.04)	0.005	0.35 (0.09)	0.55 (0.07)	0.005
Vastus medialis	0.20 (0.15)	0.21 (0.10)	0.799	0.28 (0.06)	0.31 (0.05)	0.007	0.37 (0.07)	0.39 (0.06)	0.169
Biceps femoris (LH)	0.19 (0.11)	0.23 (0.16)	0.575	0.21 (0.03)	0.22 (0.03)	0.575	0.30 (0.07)	0.32 (0.14)	0.575
Semitendinosus	0.15 (0.14)	0.21 (0.10)	0.093	0.22 (0.06)	0.28 (0.06)	0.005	0.29 (0.11)	0.36 (0.08)	0.009
Soleus	0.18 (0.11)	0.18 (0.09)	0.959	0.17 (0.06)	0.26 (0.08)	0.007	0.26 (0.09)	0.36 (0.10)	0.059
Tibialis anterior	0.17 (0.13)	0.23 (0.15)	0.721	0.26 (0.05)	0.31 (0.04)	0.005	0.32 (0.11)	0.41 (0.12)	0.114

[a]*p* value is from the Wilcoxon Signed Rank test by comparing the error from the subject-specific model with the mean error from ten scaled models ($a = 0.05$).

Table V

Correlation Between Root Mean Square Difference (RMSD) in Joint Reaction Forces From Scaled Models and the Discrepancies from the Underlying Datasets to the Modelled Subject

| | RMSD[a] | | | | | | | |
| | Ankle | | Knee | | Hip | | Sum | |
	R	*p* value	R	*p* value	R	*p* value	R	*p* value
gender[b]	*0.354*	0.001	*0.373*	<0.001	*0.355*	0.023	*0.341*	0.002
height[c]	*0.612*	<0.001	*0.585*	<0.001	*0.475*	<0.001	*0.528*	<0.001
mass[c]	*0.662*	<0.001	*0.697*	<0.001	*0.463*	<0.001	*0.550*	<0.001
limb length[c]	*0.426*	<0.001	*0.702*	<0.001	*0.536*	<0.001	*0.435*	<0.001
femur length[c]	*0.426*	<0.001	*0.585*	<0.001	*0.520*	<0.001	*0.435*	<0.001
tibia length[c]	*0.490*	<0.001	*0.658*	<0.001	*0.536*	<0.001	*0.485*	<0.001
pelvis width[c]	0.103	0.335	0.101	0.354	*0.256*	0.001	0.142	0.212
BMI[c]	*0.459*	<0.001	*0.360*	0.001	*0.401*	<0.001	*0.404*	<0.001
limb length to pelvis width ratio[c]	*0.324*	0.002	*0.441*	<0.001	*0.516*	<0.001	*0.380*	0.001

The values in italics are statistically significant.

[a]RMSDs in ankle, knee and hip joints, and the sum of these, are expressed as the percentage of mean force from the subject-specific model.

[b]Difference in gender is defined as 1 or 0.

[c]Difference in anthropometry measurements is expressed as a percentage difference from the underlying dataset to the subject; pelvis width is defined as the distance between right and left anterior superior iliac spine; the limb length to pelvis width ratio (ratio) is defined as limb length divided by pelvis width.

Table VI

Identified Multiple Regression Models to Quantify Root Mean Square Difference (RMSD) in Joint Reaction Forces

	Predictor	R	R^2	Adjusted R^2	Change in R^2	*p* value
Ankle	constant + mass	0.662	0.439	0.432	0.439	<0.001
	constant + mass+ gender	0.698	0.488	0.476	0.049	<0.001

	Multiple Regression Model	**$RMSD^a$ = 11.06+0.49× mass+7.66× gender**				
		B^b	Standard error	*p* value	95% CI^b	
	constant	11.061	2.156	<0.001	6.775	15.346
	mass	0.490	0.063	<0.001	0.365	0.615
	gender^c	7.663	2.672	0.005	2.350	12.975

	Predictor	R	R^2	Adjusted R^2	Change in R^2	*p* value
Knee	constant+ LL	0.702	0.493	0.487	0.493	<0.001
	constant+ LL+ mass	0.744	0.553	0.542	0.060	<0.001
	constant+ LL+ mass+ ratio	0.764	0.583	0.568	0.030	<0.001
	constant+ LL+ mass+ ratio+ gender	0.783	0.613	0.595	0.030	<0.001

	Multiple Regression Model	**RMSD = 5.32+1.00× LL+0.38× mass+37.22× ratio+7.75× gender**				
		B	Standard error	*p* value	95% CI	
	Constant	5.321	2.780	0.059	-0.210	10.851
	LL^d	1.001	0.411	0.017	0.184	1.819
	mass^d	0.379	0.108	0.001	0.165	0.594
	ratio^d	37.221	14.257	0.011	8.860	65.582
	gender	7.751	3.062	0.013	1.660	13.842

	Predictor	R	R^2	Adjusted R^2	Change in R^2	*p* value
Hip	constant+ LL	0.536	0.287	0.278	0.287	<0.001
	constant+ LL+ mass	0.580	0.337	0.319	0.050	<0.001
	constant+ LL+ mass+ gender	0.599	0.359	0.333	0.022	<0.001

	Multiple Regression Model	**RMSD = 9.60+0.38× LL+0.10× mass+2.64× gender**				
		B	Standard error	*p* value	95% CI	
	Constant	9.595	1.436	<0.001	6.642	12.549
	LL	0.377	8.337	<0.001	0.172	0.582
	mass	0.096	0.041	0.033	0.008	0.183
	gender	2.641	1.626	0.039	-0.634	5.917

		R	R^2	Adjusted R^2	Change in R^2	*p* value
Overall	constant+ mass	0.550	0.302	0.293	0.302	<0.001
	constant+ mass+ gender	0.602	0.363	0.346	0.061	0.009
	constant+ mass+ gender+ LL	0.629	0.396	0.372	0.033	0.046

Multiple Regression Model	RMSD = 7.40+0.16× mass+4.03× gender+0.16× ratio				
	B	Standard error	*p* value	95% CI	
Constant	7.399	1.326	<0.001	4.758	10.040
mass	0.163	0.037	<0.001	0.089	0.237
gender	4.031	1.484	0.008	1.074	6.987
ratio	0.158	0.078	0.046	0.003	0.313

[a] RMSDs from the scaled modes in joint reaction forces at the ankle, knee, hip and their sum are expressed as the percentage of mean force from the subject-specific model.

[b] B indicates regression coefficient; CI indicates confidence interval.

[c] Difference in gender is defined as 1 or 0.

[d] Difference in mass (mass), limb length (LL) and limb length to pelvis width ratio (ratio) is expressed as percentage difference from the underlying dataset to the modelled subject.

Table VII

A Comparison of Root Mean Square Difference (RMSD) and Coefficient of Determination (R^2) in Joint Reaction Forces Produced by the Scaled Generic Model and the Scaled Closest Model.

	Ankle				Knee				Hip				Sum[c]			
	Scaled-generic		Scaled-closest[a]		Scaled-generic		Scaled-closest		Scaled-generic		Scaled-closest		Scaled-generic		Scaled-closest	
	RMSD (%)	R^2	RMSD (%)	R^2	RMSD (%)	R^2	RMSD (%)	R^2	RMSD (%)	R^2	RMSD (%)	R^2	RMSD (%)	R^2	RMSD (%)	R^2
M1	20	0.99	14	0.98	55	0.64	18	0.92	32	0.86	16	0.97	25	0.83	11	0.96
M2	43	0.76	13	0.98	37	0.82	15	0.97	32	0.81	11	0.98	38	0.80	13	0.98
M3	31	0.90	15	0.99	40	0.79	20	0.97	36	0.91	21	0.94	49	0.87	10	0.97
M4	43	0.79	5	0.99	55	0.76	13	0.93	19	0.97	16	0.97	54	0.84	11	0.96
M5	87	0.81	9	0.99	56	0.75	20	0.99	39	0.92	9	0.99	31	0.82	11	0.99
F1	13	0.99	10	0.99	37	0.89	10	0.99	43	0.86	17	0.98	47	0.91	5	0.99
F2	47	0.70	35	0.96	35	0.96	14	0.90	26	0.88	22	0.94	52	0.85	10	0.94
F3	51	0.17	28	0.94	57	0.55	12	0.99	48	0.94	30	0.99	34	0.56	17	0.97
F4	40	0.76	17	0.95	44	0.75	11	0.93	37	0.83	13	0.95	52	0.78	10	0.94
F5	64	0.57	18	0.89	69	0.54	30	0.89	24	0.94	10	0.93	79	0.68	27	0.91
Mean	44	0.72	16	0.97	48	0.76	16	0.95	34	0.90	17	0.96	46	0.79	13	0.96
SD	21	0.23	9	0.03	11	0.14	6	0.04	9	0.05	7	0.02	15	0.10	6	0.02
p value[b]			0.005				0.005				0.005				0.005	

M and F designate male and female.

[a]The closest musculoskeletal model for scaling (scaled-closest) is derived from the multiple regression model with the minimum RMSD (min $f(\text{RMSD}_d)$) in joint reaction forces: for the ankle, min $f(\text{RMSD}_d)$ = min $(11.06 + 0.49 \times \text{mass}_d + 7.66 \times \text{gender}_d)$; for the knee, min $f(\text{RMSD}_d)$ = min $(5.32 + 1.00 \times \text{LL}_d + 0.38 \times \text{mass}_d + 37.22 \times \text{ratio}_d + 7.75 \times \text{gender}_d)$; for the hip, min $f(\text{RMSD}_d)$ = min $(9.60 + 0.38 \times \text{LL}_d + 0.10 \times \text{mass}_d + 2.64 \times \text{gender}_d)$; and for their sum, min $f(\text{RMSD}_d)$ = min $(7.40 + 0.16 \times \text{mass}_d + 4.03 \times \text{gender}_d + 0.16 \times \text{ratio}_d)$, where: gender_d indicates the difference in gender between the subject and the model (d), which is 1 when gender is different else is 0; mass_d, LL_d and ratio_d indicate the percentage difference in mass, limb length (LL) and the limb length to pelvis width ratio from the underlying dataset (d) to the modelled subject.

[b]p value is from the Wilcoxon Signed Rank test between RMSDs from scaled-generic and scaled-closest models ($a = 0.05$).

[c]RMSDs of the sum of joint reaction forces of ankle, knee and hip; R^2 is the mean R^2 in joint reaction forces of ankle, knee and hip.